

---

# Measurement of Preheat due to Fast Electrons in Laser Implosions of Cryogenic Deuterium Targets

## Introduction

The fraction of the incident laser energy that is deposited by energetic electrons as preheat in the cryogenic fuel of imploded spherical targets has been measured for the first time. Preheat due to fast electrons has long been identified as a contributing factor in performance degradation in laser-imploded fusion targets.<sup>1</sup> Fast-electron preheat reduces the fuel compressibility, thereby reducing the ignition margin. Theoretical designs for direct-drive fusion experiments on the National Ignition Facility (NIF)<sup>2</sup> use shock preheat to control the isentrope of the ablation surface and the fuel by varying the incident laser pulse shape. However, additional preheat due to fast electrons can be detrimental to the target gain. Detailed simulations have shown that the fraction of the laser energy dumped as total preheat in the cryogenic DT fuel has to be well below 0.1% for the preheat problem to have a negligible impact on target performance.<sup>3</sup> This fraction is the key parameter in assessing the severity of preheat and is the quantity determined in this work, based on the measured hard-x-ray (HXR) continuum on the OMEGA<sup>4</sup> laser system. In an earlier work,<sup>5</sup> the source of the fast electrons has been identified as the two-plasmon-decay instability, but the determination of preheat level is independent of this identification. Measuring the fast-electron preheat is particularly important because the calculation of the fast-electron source is difficult and is not included in most hydrodynamic target simulations. The present measurements of preheat in cryogenic-fuel targets on the OMEGA laser system are relevant to future high-gain direct-drive implosions on the NIF since the laser irradiation,  $\sim 10^{15}$  W/cm<sup>2</sup>, is similar to the design irradiance for the NIF direct-drive cryogenic targets.<sup>2</sup> Although the ablation density scale length (which affects the generation of fast electrons) is shorter than that of NIF targets, earlier experiments<sup>5</sup> on planar CH targets with scale lengths comparable to those on NIF-design targets have shown the preheat fraction to be about the same as in the present spherical experiments. Furthermore, using various combinations of phase plates and laser-beam configurations on planar targets, the experiments showed<sup>5</sup> that the total HXR signal scaled primarily with irradiance, not with scale length or plasma tempera-

ture. Thus, the present OMEGA preheat results can be projected to future direct-drive experiments on the NIF.

To calibrate the HXR detectors, a CH-coated molybdenum solid sphere was irradiated, and the HXR continuum and absolutely calibrated Mo-K $\alpha$  line were measured simultaneously. Using the relationship between these two measured quantities (through the preheat) provided a calibration of the HXR detectors. Using this calibration, we determine, first, the preheat in thick imploding CH shells filled with deuterium gas and then the preheat in cryogenic-deuterium targets. In all these cases (including the cryogenic targets) the laser interaction and, thus, the production of fast electrons occur within the outer CH layer.

The preheat level is determined directly from the measured spectrum of the hard x rays. The only required parameters are the total hard-x-ray energy and the fast-electron temperature, both obtained from the measured spectrum. This determination bypasses the need to know the trajectories or dynamics of the fast electrons: for each fast electron interacting with the target, there is a direct ratio between the cross section for slowing down collisions (which constitute preheat) and the cross section to emit continuum or K $\alpha$  radiation. Thus, the observed radiation (of either kind) leads directly to the preheat level. These assertions are strongly supported by the transport simulation results shown below.

## Preheat in Thick CH Shells

The HXR signal for a series of deuterium-gas-filled, thick CH shells as a function of laser irradiance has been published,<sup>5</sup> but without a determination of the preheat level. The CH shells were 27  $\mu\text{m}$  thick, 900 to 1100  $\mu\text{m}$  in diameter, and filled with 20 atm of deuterium gas. They were irradiated with 60 beams at 351-nm wavelength, of 1-ns square pulse, and irradiance in the range of 6 to  $9 \times 10^{14}$  W/cm<sup>2</sup>. The beam parameters specified here were also used for the molybdenum and the cryogenic targets described below. In the case of thick CH shells, the fast electrons interact mostly with cold CH. The

slowing down and radiation by electrons passing through the deuterium fill gas is negligible. We simulate the transport of fast electrons and emission of bremsstrahlung radiation within the CH by a multigroup transport code<sup>6</sup> that assumes the initial electron energy distribution function to be Maxwellian (this assumption is based on 2-D simulations of the two-plasmon-decay instability<sup>7</sup>). The number of fast electrons is immaterial for the calculation of the ratio of preheat to x-ray emission. The collisions causing the slowing down are calculated from the stopping-power and range tables of the National Institute of Standards and Technology (NIST),<sup>8</sup> which are based on Bethe's  $dE/dx$  formula<sup>9</sup> and the density correction of Sternheimer.<sup>10</sup> The energy loss rate due to bremsstrahlung is given by the Heitler relativistic formula.<sup>11</sup>

Figure 101.59 shows the results of these calculations. The curve marked "transport" is the result of transporting the multigroup distribution of initial temperature  $T$  through the total CH shell thickness. The curve marked " $dE/dx$  ratio" is the ratio of the energy-loss rates for slowing-down collisions and for bremsstrahlung emission of electrons of a single energy  $E$ . The major factor determining the shape of these curves (and their differences) is the fact that the slowing-down rate is approximately proportional to  $1/E$ . The two curves differ in two

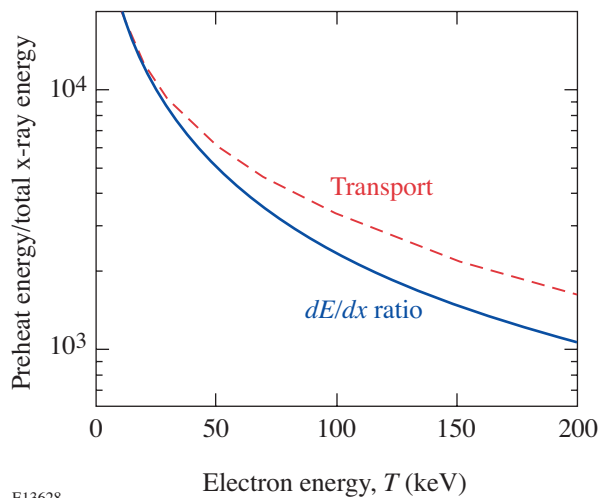


Figure 101.59  
Calculated ratio of preheat energy to total hard-x-ray energy for CH shells. The curve marked "transport" is the result of multigroup fast-electron transport through the 27- $\mu\text{m}$ -thick shell, for an initially Maxwellian distribution of temperature  $T$ . The curve marked " $dE/dx$  ratio" is the ratio of the energy-loss rates for stopping-power collisions and for bremsstrahlung emission for electrons of a single energy  $E$ . The abscissa values for the two curves refer to fast-electron temperature (for the transport curve) and electron energy (for the  $dE/dx$ -ratio curve).

respects: the transport curve is the result of integration over the thickness of the target and it refers to an initially Maxwellian energy distribution, whereas the  $dE/dx$  curve refers to the local rates and to a single energy. At the limit of very high temperature, where transport is unimportant, the second factor dominates: since in a Maxwellian energy spectrum there are more electrons below the energy  $E = T$  (where the slowing-down rate is higher) than above it, the preheat for the transport curve is higher than for the  $dE/dx$ -ratio curve. For lower temperatures the same effect dominates only in a thin layer below the target surface; farther in, more and more of the slow electrons lose all their energy and the distribution is left with only higher-energy electrons, for which the slowing-down rate is lower.

The purpose of comparing the two curves in Fig. 101.59 is to show that the role of scattering (which was neglected here) is relatively unimportant for the calculation of the ratio of preheat to x-ray emission. Thus, the  $dE/dx$  ratio can be viewed as the result of transport in the limit of a very thin shell for which scattering is negligible. The inclusion of scattering in the transport, by extending the electron paths, would increase both the preheat and the HXR energy by the same factor. Furthermore, varying the shell thickness leaves the ratio of preheat to total HXR energy virtually unchanged, which again supports the omission of scattering. An additional confirmation of this assertion is provided by the molybdenum results below. Thus, by relating the preheat to the observed HXR signal, we bypass all questions related to the fast-electron paths. The slowing down from the NIST tables pertains to cold material. This assumption is true for most of the CH shell throughout the duration of the laser pulse. Furthermore, using a slowing-down formula for ionized material yields only slightly different results (see below). Thus, using the NIST tables for the total CH shell is adequate. The transport curve in Fig. 101.59 is used to determine the preheat fraction for the imploding CH shells. The fast-electron temperature for each target shot was determined from the slope of the HXR spectrum;<sup>5</sup> for the narrow range of laser irradiance  $I \sim 6$  to  $9 \times 10^{14}$  W/cm<sup>2</sup>, the fast-electron temperature changes in the range of 60 to 80 keV. The temperature was determined<sup>5</sup> with a precision of  $\pm 15\%$ , which translates to a precision of about  $\pm 10\%$  in the preheat fraction in this temperature range.

To determine the preheat energy, the HXR energy must be measured absolutely. To that end, we irradiated a CH-coated molybdenum solid sphere where the preheat was measured simultaneously through the HXR continuum and the (absolutely calibrated) Mo-K $\alpha$  line. Most of the HXR emission

(and all the  $K\alpha$  emission) comes from the molybdenum. Molybdenum was chosen to minimize the contribution of thermal x rays to the excitation of the  $K\alpha$  line. Previous experiments on planar targets<sup>6</sup> with  $K\alpha$  lines of energy around 5 keV showed that the contribution of radiation to the production of  $K\alpha$  lines was comparable to that of fast electrons (in all cases the laser interacts only with the CH coating). To differentiate between the two contributions, dual-element (V and Ti) targets were used, and the  $K\alpha$  lines were observed from both sides of the target. Since that solution is not available with spherical targets, we chose a much-higher- $Z$  element. Only radiation above the Mo-K edge, at 20 keV, can contribute to the excitation of the Mo- $K\alpha$  line. At that energy, the thermal x-ray spectrum is several orders of magnitude lower than at 5 keV. Figure 101.60 shows a film lineout of the  $K\alpha$  line of molybdenum from a CH-coated molybdenum sphere. The target consisted of a 1.07-mm-diam Mo sphere coated with 12  $\mu\text{m}$  of CH and was irradiated at  $7.7 \times 10^{14}$  W/cm<sup>2</sup>. As expected, the continuum intensity underlying the  $K\alpha$  line is too weak to measure. This confirms the assertion that the  $K\alpha$  line is excited exclusively by fast electrons (neither can it be excited by the hard x rays, whose energy is found to be lower than that of the  $K\alpha$  line).

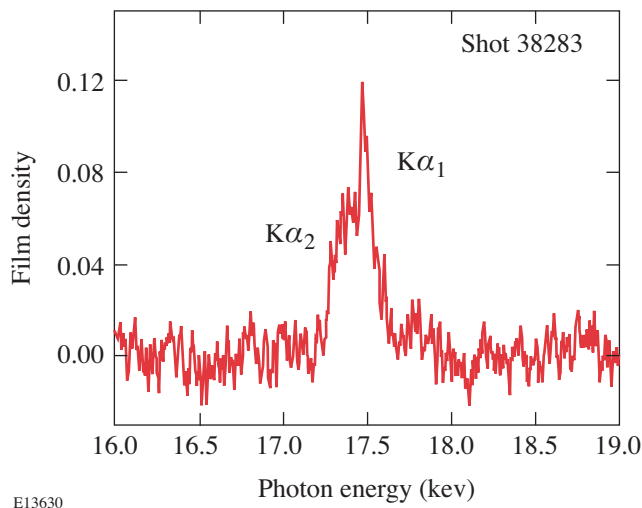


Figure 101.60  
Measured  $K\alpha$  line of molybdenum from CH-coated molybdenum sphere.

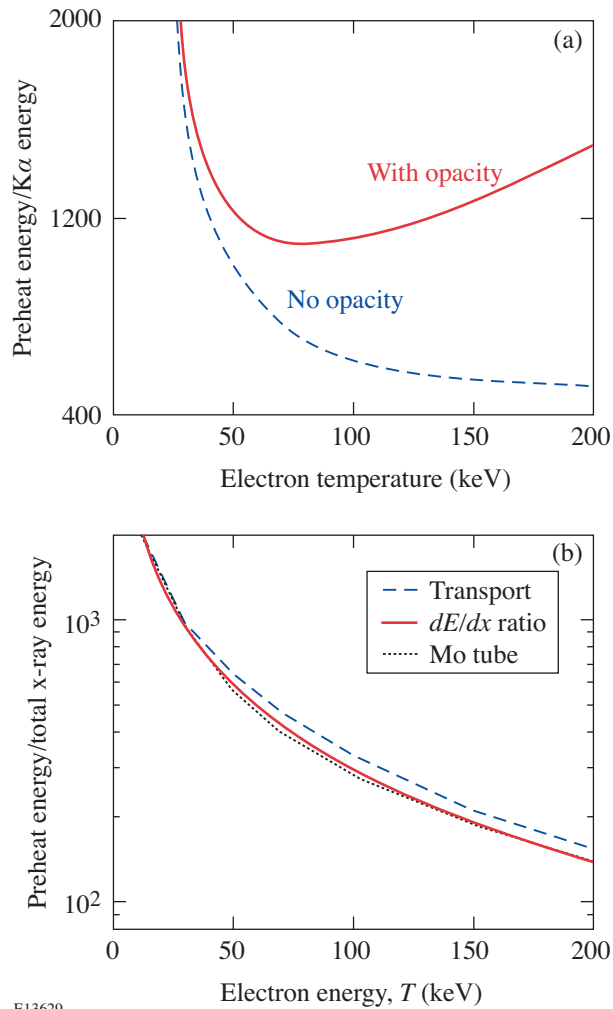
The measured  $K\alpha$  line on film is converted to energy using the crystal and film calibrations. For the crystal used [polished and etched LiF (2,0,0)], our calibration<sup>12</sup> agrees well with the results of Toh *et al.*<sup>13</sup> and Gilfrich *et al.*<sup>14</sup> The published calibration for the Kodak direct-exposure film (DEF) was used<sup>15</sup> with the film-processing procedure closely followed. Above the Br K edge (at 13.475 keV) the film density is almost

exactly linear with x-ray flux, which greatly simplifies the film conversion. The total energy emitted by the target in the  $K\alpha$  line per unit solid angle is given by  $E_l L/R$ , where  $E_l$  is the energy incident on the film per unit length along the line,  $R$  is the crystal integrated reflectivity at the  $K\alpha$  energy, and  $L$  is the distance from target to film along the spectral ray.

To relate the intensity of the Mo- $K\alpha$  line to the fast-electron energy, we use the multigroup code for the transport of the fast electrons with the inclusion of the rate for excitation of the  $K\alpha$  line. The photoionization rate of K-shell electrons, which leads to  $K\alpha$  emission, is given by the semi-empirical cross section of Powell.<sup>16</sup> In addition, the code calculates the transport of the  $K\alpha$  line emission out of the target. The results, with and without the inclusion of the  $K\alpha$  opacity, are shown in Fig. 101.61(a). Using the curve marked “with opacity” and the measured  $K\alpha$  emission, the preheat can be determined. The HXR emission in molybdenum is calculated in the same way as for the CH targets, and the results are shown in Fig. 101.61(b). As in Fig. 101.59, the abscissa designates electron temperature for the transport curve and electron energy for the  $dE/dx$ -ratio curve.

We can gain additional confidence in the curves of Fig. 101.61(b), and, by implication, those of Fig. 101.59, by comparing them with the known efficiency  $\varepsilon$  of an x-ray tube with a molybdenum anode. The input power that accelerates the electrons in the tube is converted mainly to heating the anode (equivalent to preheat in our case), with a small fraction converted to x rays, mostly continuum. The power  $P$  of x-ray continuum emission is given by the empirical relation<sup>17</sup>  $P = K(Z) \times Z \times I \times V^2$ , where  $V$  and  $I$  are the accelerating voltage and the tube current, respectively, and  $K$  depends weakly on the atomic charge  $Z$ . Thus, the ratio of heating to radiation is  $\varepsilon^{-1} = [Z \times V \times K(Z)]^{-1}$ . For molybdenum, the empirical value<sup>17</sup> of  $K$  is  $\sim 0.85 \times 10^{-6}$  keV<sup>-1</sup>. Plotting  $\varepsilon^{-1}$  as a function of  $V$  results in the dotted curve for the Mo tube in Fig. 101.61(b) (where the electron energy is given by  $V$ ). Good agreement with the theoretical curves is seen. This provides an additional confirmation that the modeling of preheat-to-radiation ratio, in particular the neglect of scattering, is correct.

Using both Figs. 101.61(a) and 101.61(b) for the same molybdenum target shot, we derive the calibration of the HXR detector against the absolute energy of the Mo- $K\alpha$  line. The resulting calibration, in units of x-ray energy per electrical charge of the time-integrated HXR signal, is  $C = 0.018$  mJ/pC. This calibration factor depends weakly on the fast-electron temperature. To determine this dependence, we averaged the



E13629

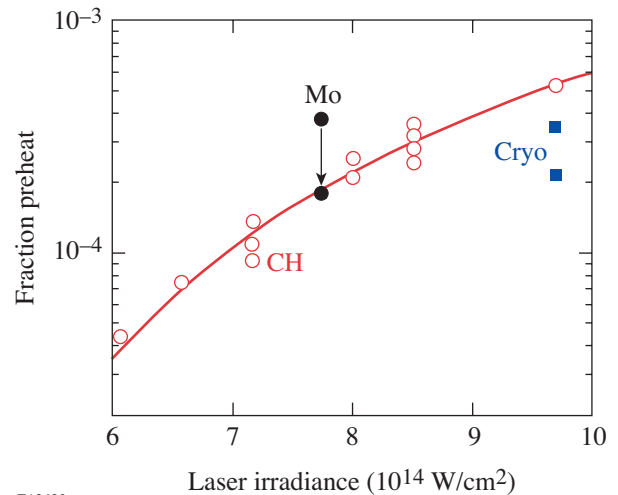
Figure 101.61

Calculations for a molybdenum target. (a) Ratio of preheat energy and emission energy in the  $\text{Mo-K}\alpha$  line, calculated by a multigroup electron transport through a molybdenum sphere. The curve marked "with opacity" includes the transport of the  $K\alpha$  line through the target. (b) The transport curve (dashed) and the  $dE/dx$  ratio curve (solid) are equivalent to the two curves in Fig. 101.59. The dotted curve is the inverse of the empirical x-ray efficiency of an x-ray tube with a Mo anode (the abscissa for the latter curve is given by the tube voltage).

relative detector sensitivity<sup>18</sup> over the HXR spectrum for each temperature. The uncertainty in the calibration factor is determined by that of the  $K\alpha$  energy, which is estimated to be  $\pm 20\%$ . This adds to the effect of temperature uncertainty discussed above to yield a total uncertainty in the preheat of  $\pm 30\%$ .

The final values of preheat as a fraction of the laser energy for the thick ( $27\text{-}\mu\text{m}$ ) CH shells are shown as open circles in

Fig. 101.62. Also shown as a solid circle marked "Mo" is the preheat in the CH-coated molybdenum target. In that case, the preheat energy can be equated with the initial energy in fast electrons that travel through the target since their range is much smaller than the radius of the molybdenum sphere and almost all the incident energy is converted to preheat. This energy can also be equated with the initial energy  $E_{\text{init}}$  in fast electrons that travel through a  $27\text{-}\mu\text{m}$ -thick CH shell at the same irradiance ( $I_0 = 7.7 \times 10^{14} \text{ W/cm}^2$ ) since, in the two cases, a laser of the same irradiance and pulse shape interacts with a spherical CH layer of the same radius. For the measured fast-electron temperature at irradiance  $I_0$ , the transport code calculates the fraction of  $E_{\text{init}}$  absorbed as preheat when an electron distribution of temperature  $T$  travels through a  $27\text{-}\mu\text{m}$ -thick CH shell. The result is shown by the solid circle at the end of the arrow, and it agrees with the measured preheat for CH shells (i.e., it lies on the curve). This agreement indicates that the fast electrons traverse the shell only once, otherwise the point would lie below the curve. The possible reflection of electrons back into the target, due to a surrounding electric field, is an important factor in the study of fast-electron dynamics. The question of reflection, however, is not germane to the determination of the preheat level.



E13632

Figure 101.62

Preheat energy as a fraction of the incident laser energy deduced from the hard-x-ray measurements. Open circles: deuterium-gas-filled thick CH shells; point marked "Mo": CH-coated molybdenum sphere; solid squares: cryogenic-deuterium-filled CH shells. For the point at the end of the arrow see the text.

### Preheat in Cryogenic Targets

A series of laser implosion experiments of cryogenic-deuterium targets were conducted recently and are described

in detail in Ref. 19. The preheat level for a few typical shots from this series was determined based on the HXR measured signals. The targets were  $\sim 3.5\text{-}\mu\text{m}$ -thick CH shells, filled with about 1000 atm of deuterium, which upon solidification yielded  $\sim 100\text{-}\mu\text{m}$ -thick solid deuterium layer on the inner surface of the CH shell. The laser energy was  $\sim 22.6$  kJ in a 1-ns square pulse. Other details (target quality, etc.) are discussed in Ref. 19.

The determination of preheat in cryogenic targets is more involved than that for thick CH shells. First, because the cryogenic fuel is not cold, the formula for electron slowing down in a plasma rather than in a cold material must be used. Furthermore, most of the measured HXR signal is emitted by the CH layer, not the DD fuel. This is in spite of the fact that most of the electron slowing down occurs in the deuterium fuel. Therefore, to find the fraction of the HXR signal coming from the fuel, the successive transport of electrons through the CH and fuel layers is computed.

The slowing down of electrons in a plasma has two contributions: binary collisions and collective interactions (i.e., excitation of plasma waves). In the kinetic formulations of the problem, the division between the two regimes is marked by an impact parameter that is smaller or larger than the Debye length  $L_D$ . In the continuum (or dielectric) formulations of the problem, the division is marked by a density modulation wave number  $k$  that is larger or smaller than  $k_D = 1/L_D$ . The effect of the plasma ions is negligible for the high projectile velocities considered here.<sup>20</sup> The addition of the two electron collision terms for high projectile velocities yields<sup>20</sup>

$$(-dE/dx) = (2\pi e^4 N_e / E_0) \ln(1.52 E_0 / \hbar \omega_p),$$

where the plasma frequency is given by  $\omega_p = (4\pi e^2 N_e / m)^{1/2}$ . The Debye length dependence has canceled out because the argument of the logarithm in the binary-collision term is  $(L_D / 1.47 b_{\min})$ , where  $b$  is the impact parameter, whereas in the collective-collision term it is  $(1.123 V_0 / \omega_p L_D)$ , where  $V_0$  is the projectile velocity; thus, by adding the two terms, the Debye length cancels out. This is an indication that the result is independent of the degree of degeneracy, which was also shown directly by Maynard and Deutsch.<sup>21</sup> The issue of using single-particle slowing-down formulas in this work was addressed in detail in the Appendix of Ref. 6; the main justification for neglecting collective effects is that the preheat is measured from HXR emission rather than deduced from the motion of the electrons that produce it. The result is very similar to the Bethe stopping-power formula<sup>9</sup> with the main

difference being that the average ionization energy in the Bethe formula is replaced by  $\hbar \omega_p$ . For the deuterium fuel used in these experiments, the two equations yield very similar results.

The transport of electrons in these targets is calculated using the density profiles calculated by the one-dimensional (1-D) *LILAC* hydrodynamic code.<sup>22</sup> Throughout the laser pulse, the quarter-critical density surface (the region where the fast electrons are generated) remains within the CH layer. The fraction of the total HXR signal emitted by the deuterium fuel increases slightly during the laser pulse. The time-integrated HXR emission from the fuel is  $\sim 1/4$  of the total HXR signal. The transport through the fuel layer can be used to generate preheat curves similar to those of Figs. 101.59 and 101.60(b), for various assumed fast-electron temperatures. Figure 101.63 shows the energy ratio of preheat and HXR computed for two instances during the laser pulse. The ratio is seen to change very little during the laser pulse. It also changes very little if the *LILAC* density profiles are replaced by constant-density profiles of the same total mass. Thus, because the preheat and HXR depend mostly on the areal density of material traversed (in addition to the number and spectrum of the fast electrons), the results are relatively insensitive to the precision of 1-D code simulations. Finally, the resulting preheat level for two cryogenic shots is shown as solid squares in Fig. 101.62. The results for all other cryogenic targets in this series (all at about the same laser irradiance) fall within the range spanned by

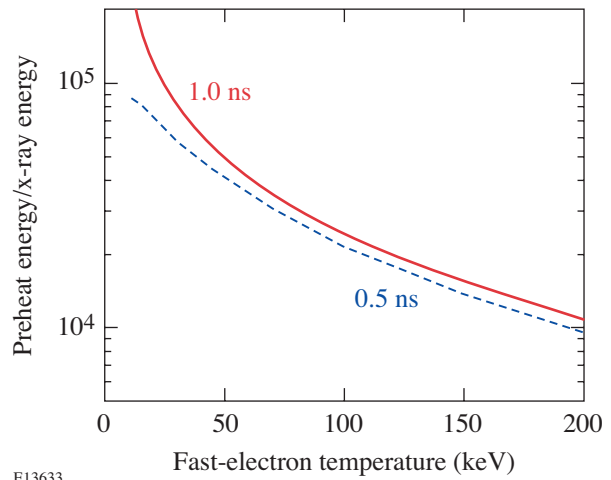


Figure 101.63

Calculated ratio of preheat energy and total hard-x-ray energy in the cryogenic-deuterium fuel. The electron transport code used the electron-density profiles calculated by *LILAC*. Shown is the ratio at two instances during the 1-ns laser pulse.

these two points. The preheat in the cryogenic fuel is smaller than that in the thick CH shells mainly because the electron areal density in the former is  $\sim 1/3$  smaller than that in the latter.

As seen in Fig. 101.62, the preheat fraction is well below 0.1%. This indicates that preheat in these cryogenic target implosions will have a negligible impact on target performance. Since direct-drive target designs employ some shock preheating to reduce the growth of hydrodynamic instability (by adjusting the laser pulse shape), a reduction of the designed shock heating level could compensate for the preheat due to fast electrons. As explained in the introduction, these considerations are expected to hold equally for future direct-drive experiments on the NIF.

#### ACKNOWLEDGMENT

This work was supported by the U.S. Department of Energy Office of Inertial Confinement Fusion under Cooperative Agreement No. DE-FC52-92SF19460, the University of Rochester, and the New York State Energy Research and Development Authority. The support of the Department of Energy (DOE) does not constitute an endorsement by DOE of the views expressed in this article.

#### REFERENCES

1. J. D. Lindl, *Inertial Confinement Fusion: The Quest for Ignition and Energy Gain Using Indirect Drive* (Springer-Verlag, New York, 1998), Chap. 11.
2. P. W. McKenty, V. N. Goncharov, R. P. J. Town, S. Skupsky, R. Betti, and R. L. McCrory, *Phys. Plasmas* **8**, 2315 (2001).
3. Laboratory for Laser Energetics LLE Review **79**, 121, NTIS document No. DOE/SF/19460-317 (1999). Copies may be obtained from the National Technical Information Service, Springfield, VA 22161.
4. T. R. Boehly, R. S. Craxton, T. H. Hinterman, J. H. Kelly, T. J. Kessler, S. A. Kumpan, S. A. Letzring, R. L. McCrory, S. F. B. Morse, W. Seka, S. Skupsky, J. M. Soures, and C. P. Verdon, *Rev. Sci. Instrum.* **66**, 508 (1995).
5. C. Stoeckl, R. E. Bahr, B. Yaakobi, W. Seka, S. P. Regan, R. S. Craxton, J. A. Delettrez, R. W. Short, J. Myatt, A. V. Maximov, and H. Baldis, *Phys. Rev. Lett.* **90**, 235002 (2003).
6. B. Yaakobi, C. Stoeckl, T. Boehly, D. D. Meyerhofer, and W. Seka, *Phys. Plasmas* **7**, 3714 (2000).
7. A. B. Langdon, B. F. Lasinski, and W. L. Kruer, *Phys. Rev. Lett.* **43**, 133 (1979).
8. M. J. Berger, J. S. Coursey, and M. A. Zucker, *ESTAR, PSTAR, and ASTAR: Computer Programs for Calculating Stopping-Power and Range Tables for Electrons, Protons, and Helium Ions* (version 1.2.2). [Online] Available: <http://physics.nist.gov/Star> [2005, February 25]. National Institute of Standards and Technology, Gaithersburg, MD.
9. H. Bethe, *Ann. Phys.* **5**, 325 (1930); *Z. Phys.* **76**, 293 (1932).
10. R. M. Sternheimer, *Phys. Rev.* **88**, 851 (1952).
11. W. Heitler, *The Quantum Theory of Radiation*, 2nd ed., The International Series of Monographs on Physics (Oxford University Press, London, 1947).
12. A. J. Burek and B. Yaakobi, *Final Report to the National Bureau of Standards Contract NB81NAHA2032*, Appendix A, NTIS document No. DE83015439 (1983). Copies may be ordered from the National Technical Information Service, Springfield, VA 22161.
13. K. Toh, T. Ui, and E. Asada, in *Advances in X-Ray Analysis*, edited by C. S. Barrett, P. K. Predecki, and D. E. Leyden (Plenum Press, New York, 1985), Vol. 28, pp. 119–126.
14. J. V. Gilfrich, D. B. Brown, and P. G. Burkhalter, *Appl. Spectrosc.* **29**, 322 (1975).
15. B. L. Henke, E. M. Gullikson, and J. C. Davis, *At. Data Nucl. Data Tables* **54**, 181 (1993).
16. C. J. Powell, *Rev. Mod. Phys.* **48**, 33 (1976).
17. N. A. Dyson, *X-Rays in Atomic and Nuclear Physics*, 2nd ed. (Cambridge University Press, Cambridge, England, 1990), p. 47.
18. C. Stoeckl, V. Yu. Glebov, D. D. Meyerhofer, W. Seka, B. Yaakobi, R. P. J. Town, and J. D. Zuegel, *Rev. Sci. Instrum.* **72**, 1197 (2001).
19. P. W. McKenty, T. C. Sangster, M. Alexander, R. Betti, R. S. Craxton, J. A. Delettrez, L. Elasky, R. Epstein, A. Frank, V. Yu. Glebov, V. N. Goncharov, D. R. Harding, S. Jin, J. P. Knauer, R. L. Keck, S. J. Loucks, L. D. Lund, R. L. McCrory, F. J. Marshall, D. D. Meyerhofer, S. P. Regan, P. B. Radha, S. Roberts, W. Seka, S. Skupsky, V. A. Smalyuk, J. M. Soures, K. A. Thorp, M. Wozniak, J. A. Frenje, C. K. Li, R. D. Petrasso, F. H. Séguin, K. A. Fletcher, S. Padalino, C. Freeman, N. Izumi, J. A. Koch, R. A. Lerche, M. J. Moran, T. W. Phillips, G. J. Schmid, and C. Sorce, *Phys. Plasmas* **11**, 2790 (2004).
20. J. D. Jackson, *Classical Electrodynamics* (Wiley, New York, 1962).
21. G. Maynard and C. Deutsch, *Phys. Rev. A, Gen. Phys.* **26**, 665 (1982).
22. R. Epstein, S. Skupsky, and J. Delettrez, *J. Quant. Spectrosc. Radiat. Transfer* **35**, 131 (1986).